

pubs.acs.org/NanoLett Letter

Nucleation Kinetics and Structure Evolution of Quasi-Two-Dimensional ZnO at the Air—Water Interface: An *In Situ* Time-Resolved Grazing Incidence X-ray Scattering Study

Ziyi Zhang, Corey Carlos, Yizhan Wang, Yutao Dong, Xin Yin, Lazarus German, Kelvin Jordan Berg, Wei Bu, and Xudong Wang*



ABSTRACT: The design and synthesis of high-quality two-dimensional (2D) materials with desired morphology are essential for property control. One critical challenge that impedes the understanding and control of 2D crystal nucleation and growth is the inability of direct observation of the nanocrystal evolution process with high enough time resolution. Here, we demonstrated an *in situ* X-ray scattering approach that directly reveals 2D wurtzite ZnO nanosheet growth at the air—water interface. The time-resolved grazing incidence X-ray diffraction (GID) and grazing incidence X-ray off-specular scattering (GIXOS) results uncovered a lateral to vertical growth kinetics switch phenomenon in the ZnO nanosheet growth. This switch represents the 2D to three-dimensional (3D) crystal structure evolution, which governs the size and thickness of nanosheets, respectively. This phenomenon can guide 2D nanocrystal synthesis with rationally controlled size and thickness. Our work opens a new pathway toward the understanding of 2D nanomaterial growth kinetics based on time-resolved liquid surface grazing incidence X-ray techniques.

KEYWORDS: Grazing incidence X-ray, In situ characterization, Liquid—air interface, Two-dimensional nanomaterials, Growth kinetics

wo-dimensional (2D) nanomaterial is one of the most popular nanoscale structures owing to its large surface-tovolume ratio and unique chemical and physical properties.^{1,2} The outstanding properties related to many critical scientific and technology disciplines, such as information systems,³ sensing,⁴ optics,⁵ energy harvesting,^{6,7} and storage,⁸ are direct results of their novel morphologies and structures. Therefore, it is essential to control the phase, crystal structure, and size of the 2D nanomaterials to achieve desired properties and applications. Although the correlations between material structure and property have been investigated widely, the atomic scale crystallization kinetics of the 2D nanocrystals are still largely uncovered. Nucleation and growth of nanocrystals usually take place only in a few seconds. Metal ion transfer and interfacial chelation happen even faster in a time scale of subseconds. Therefore, a fast in situ method for looking into the kinetics has become one of the central goals in modern kinetics studies. Nevertheless, it is still very challenging to

GID

probe these processes in real-time. Recent developments of the liquid interface grazing incidence X-ray scattering techniques ⁹⁻¹² bring new promises to time-resolved and surface-sensitive measurements, providing a capability for the studies of nucleation and mineralization from the liquid phase. ¹³ The 1D-pinhole grazing incidence X-ray diffraction (GID) can obtain in-plane angle scattering within as short as a few seconds. Grazing incidence X-ray off-specular scattering (GIXOS) can collect the vertical surface structure factors comparable to X-ray reflectivity over a much shorter period

ZnO NSs

Received: January 25, 2022 Revised: March 24, 2022 Published: March 31, 2022

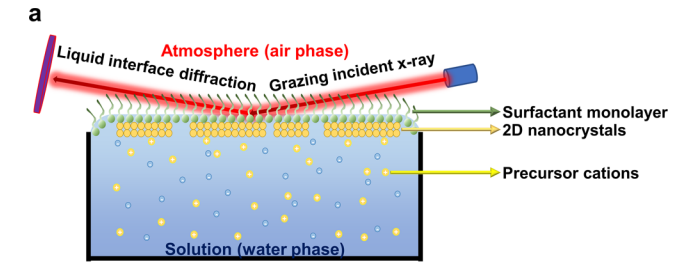




down to a subminute scale. The combination of these technologies makes time-resolved studies of fast kinetics feasible.

The ionic layer epitaxy (ILE) growth technique¹⁴ is a new solution-based synthesis approach to the formation of 2D nanomaterials. Many crystalline metal oxides have been obtained by ILE with thicknesses varied from subnanometer to a few nanometers (e.g., Bi_2O_3 , 6 CeO_2 , 15 La_2O_3 , 16 MnO_2 , 18 NiO, ¹⁴ ZnO, ¹⁴ etc.). Moreover, large-scaled crystalline noble metals, ^{17,18} hydroxides, ^{19,20} and sulfides have also been synthesized through this technique. Fundamentally, this strategy has no restriction on the intrinsic crystal structure of targeting materials and thus provides a very versatile platform for synthesizing 2D nanomaterials, particularly from those that do not have a layered structure. In addition, ILE offers an excellent platform for studying the 2D growth kinetics due to its water-based growth environment, which does not require high vacuum or high pressure. The unique 2D growth phenomenon at the air-water interface allows direct in situ observation via the liquid interface X-ray scattering techniques. It may serve as a representative system for understanding the 2D confined nucleation and growth kinetics in an aqueous environment. In this work, we present a new approach to study the 2D crystal nucleation and growth kinetics by using the time-resolved in situ grazing incidence X-ray scattering technique at the water-air interface. On the basis of the ZnO nanosheet (NS) ILE system, we uncovered the entire nucleation and growth process of the NSs by in situ GID and GIXOS. These results confirmed that the charged surfactant monolayer plays a significant role at the nucleation stage and the early crystal growth stage, where it generates a Zn²⁺ concentrated zone and lower nucleation energy sites to facilitate the 2D morphology of the oxide nanocrystals at the water-air interface. In addition, this analysis also brings knowledge of how the surfactant density, precursor concentration, and temperature affect the 2D growth. The timeresolved grazing incidence X-ray scattering technique may become a powerful strategy to study the 2D nanomaterial formation kinetics and controlling parameters.

To achieve in situ monitoring of the entire process of the ILE ZnO NS growth, an in situ ILE growth chamber was developed and integrated with the online liquid interface scattering instrument, as shown in Figure 1. A convex liquid surface was created above the trough edge, where a monolayer of sodium oleylsulfate (SOS) is formed to direct the crystallization of ZnO NS underneath, from which the GID signals were collected in real-time (more details are included in Supporting Information Section 1) The GID images taken in a time sequence during ZnO NS synthesis are shown in Figure 2. Only two diffraction peaks were observed in the GID: a diffraction rod (Bragg's rod^{21,22}) at $Q_{xy} = 2.312 \text{ Å}^{-1}$ came first (@42 min) and a diffraction ring at $Q_{xy} = 2.224 \text{ Å}^{-1}$ appeared later (@64 min). These two peaks correspond to the surface (2D) and bulk (three-dimensional, 3D) lattice spacing between wurtzite ZnO (1010) planes, respectively. As the reaction time progressed, the intensity of the diffraction rod only slightly increased, and the diffraction ring became much brighter. This indicated that ZnO nucleation was directed by the surfactant monolayer into 2D morphology at the early stage and the 3D growth occurred later to make the ZnO NS thicker. No other diffractions showed up because the NS growth was confined in a few nanometers thick, near-surface region over the growth period. On the contrary, without the



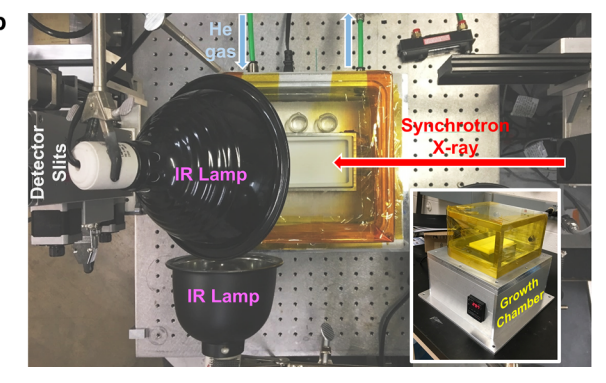


Figure 1. (a) Schematic for the *in situ* investigation of ILE ZnO NS growth at the air—water interface with grazing incidence synchrotron X-ray. (b) Experimental apparatus on Sector 15, NSF's ChemMatCARS, at Advanced Photon Source, Argonne National Lab.

surfactant monolayer, the intensity of the initial diffraction rod at $Q_{xy} = 2.312 \text{ Å}^{-1}$ reduced rapidly as the diffraction rings showed up, while a set of powder diffraction rings appeared and increased at $Q_{xy} = 2.22$, 2.42, and 2.53 Å⁻¹, which can be indexed to $(10\overline{10})$, (0002), and $(10\overline{11})$ planes, respectively (Figure 2b). In this case, the Zn²⁺ ions nucleated into 3D morphology and grew isotropically into wurtzite nanoparticles (NPs) at the water—air interface. There was no peak position shifting during the entire growth process with or without the presence of a surfactant monolayer, indicating no observable phase transform or strain relaxation happened in the crystalline domains (Figure S2). The wurtzite ZnO nanostructure was preserved over the entire nucleation and crystal growth process.

The role of the charged surfactant monolayer in the 2D ZnO nucleation was revealed by these GID results. On the basis of the intensity changes of the diffraction rod and ring, we could divide the morphologies of ZnO NSs during the growth into three categories: nucleation (tiny nuclei), 2D dominant (thin NSs), and 3D dominant (thick NSs). A series of SEM images from the *ex situ* synthesis of ZnO NSs also confirmed the crystal nucleation and 2D to 3D structure evolution from the *in situ* observations. Figure 2c—e showed ZnO NS morphologies within different regimes: tiny nuclei (@15 min), small thin triangles with a rough surface (@30 min), and large thick triangles with a flat surface (@60 min). Without the SOS monolayer, only congregated ZnO NPs formed over 120 min (Figure 2f).

The peak intensity was quantified as the integration of all the diffracted X-ray photons that have been detected, giving the total amount of the crystalline domains at the water—air interface (Supporting Information Section 2). The derived time profile of the GID intensities from the ILE ZnO NS synthesis is shown in Figure 3a. The difference between the 2D and 3D diffractions illustrated the entire crystallization process in the ILE. No peaks were shown in the first 20 min of the

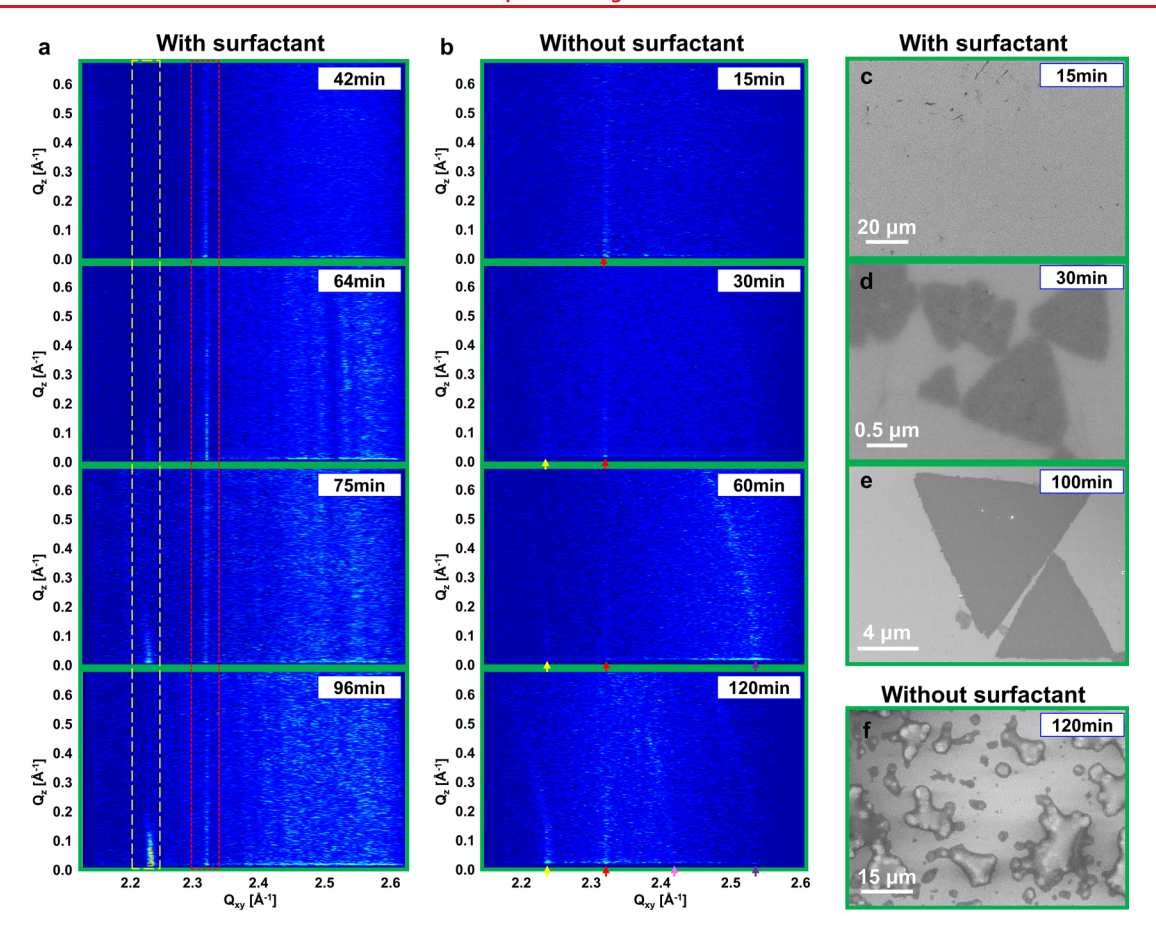


Figure 2. (a) In situ GID of ILE ZnO NS growth with surfactants. The surface diffraction (2D) signal located at $Q_{xy} = 2.312 \,\text{Å}^{-1}$ (in red dotted line box) and the bulk diffraction (3D) signal located at $Q_{xy} = 2.224 \,\text{Å}^{-1}$ (in yellow dashed line box) [measurements were done at 60 °C with 1 mM Zn²⁺]. (b) In situ GID of ZnO NP growth without surfactants. Without introducing surfactant, the diffraction ring patterns indicated the ZnO crystal grew into particles [measurements were done at 60 °C with 25 mM Zn²⁺]. (c–e) SEM images of ZnO NSs after 15, 30, and 100 min synthesis at 60 °C with surfactants. (f) SEM image of the ZnO NPs after 120 min synthesis at 60 °C without surfactants.

growth since no ordered structures were formed yet in this incubation period. Precursor ions were concentrated in the interfacial double layer to initialize the nucleation similar to the classic LaMer model. ^{23,24} The diffraction rod began to appear at 20 min and approached its maximum intensity at ~65 min, suggesting that nuclei expansion was initially directed by the surfactants at the interface and the surfactant monolayer was gradually occupied by the NSs. The diffraction ring appeared later than the rod, at 53 min, and its intensity kept increasing linearly with a relatively high rate. This suggests that the initial 2D crystals were now grown through a layer-by-layer mode, while the NSs were getting thicker. 25,26 These two curves crossed at ~75 min, which could be considered as a critical point where the amount of bulk atoms gets close to the surface atoms, and the NS structure switched from 2D to 3D (quasi-2D). This 2D-3D crystal evolution was shown by taking the ratio of the two diffractions from which the ZnO NS morphologies could be fitted into three regimes: nucleation (0-20 min), 2D dominant (20-75 min), and 3D dominant (>75 min). There was also a 2D-only regime (20-53 min) in the 2D dominant regime, where all atoms in the crystal are surface atoms.

GIXOS was applied to monitor the thickness changes of the ZnO NSs during growth, and the result is presented in Figure 3b (Supporting Information Section 3). At 1 mM $\rm Zn^{2+}$ concentration, the NS thickness became detectable at 36 min

when the thickness was 2 unit cells of wurtzite ZnO (\sim 13 Å), corresponding to the time when the diffraction rod in GID became observable. When the diffraction ring was first shown in GID (53 min), NSs had a thickness of 3 unit cells (\sim 16 Å), showing the inner lattice got back to the bulk value. Thickness was slowly increased with a linear trend until ~25 Å after 100 min when the system reached an equilibrium. At the critical 2D-3D switching time (75 min), the NS thickness was 4 atomic layers (\sim 21 Å). This suggests that only the atoms in the first two layers have the compressed in-plane lattice spacing, which could be considered as surface atoms. The atoms in the deeper layers have an in-plane lattice spacing that equals the bulk values of wurtzite ZnO (PDF#36-1451). Thus, these Xray scattering techniques clearly revealed both in-plane and out-of-plane structure changes in situ during the nucleation and growth of ILE ZnO NSs with a time resolution of 3-6 min.

In addition to the growth time, several key growth parameters were also studied by the *in situ* approaches to obtain a comprehensive understanding of how to rationally control the NS growth kinetics. By using 24 μ L of SOS surfactant solution, 25 mM precursor Zn²⁺ concentration, and 60 °C solution temperature as the original growth conditions, we only changed one parameter from the origin in each set of syntheses. The GID intensity and the full width at half the maximum (fwhm) of diffraction rods at different surfactant amounts and precursor concentrations were summarized in

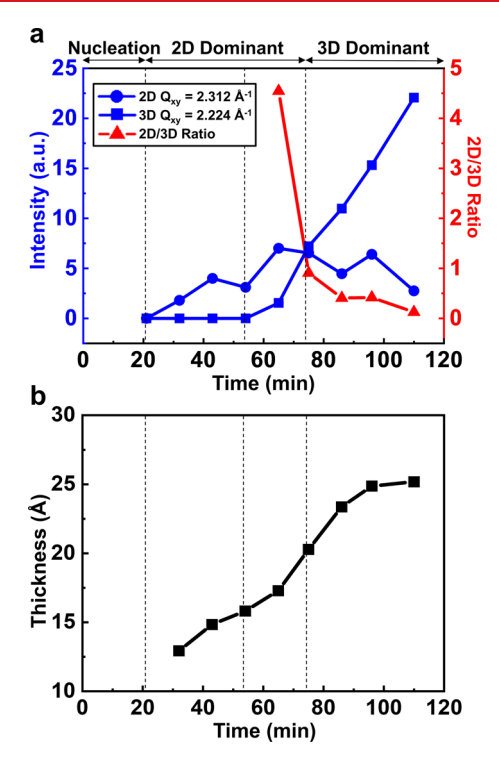


Figure 3. (a) GID intensity contours of the diffraction rod (2D) and ring (3D) for ZnO NS growth. (b) ZnO NS thickness contour during the crystal growth [measurement was done at 60 $^{\circ}$ C with 1 mM Zn²⁺].

Figure 4. When the other parameters were kept consistent, a higher surfactant concentration raised the packing density of the SOS molecules in the monolayer and enhanced the electric field at the air—water interface. The denser surfactant monolayer showed a higher peak intensity given by a faster nucleation and crystallization rate (Figure 4a). Intensity reached a maximum as the surfactant monolayer was occupied by the 2D nanocrystal formation and, thereby, ceased the

nucleation. Therefore, more surfactants could lead to a longer nucleation period. Samples with 24 and 48 μ L of SOS have similar domain sizes that were slightly smaller than the size obtained from the 72 μ L SOS samples (Figure 4b). Closer SOS packing facilitated the long-range ordering in the formation of the HCP surface structure during the 2D growth and improved the crystallinity of the ZnO NSs.

The thickness growth gave an obvious two-step behavior with two linear stages following the surfactant density (Figure 4c). The thickness increased slowly in the early growth stage and then speeded up after a certain critical point. All the three surfactant densities gave similar slopes in each stage, and the NSs from 48 μ L of SOS were slightly thinner. When one assumed the surfactants were only packed in a monolayer at the entire water surface, its packing density was estimated by dividing the total number of SOS molecules over the trough surface area (Supporting Information Section 4). When the GID and GIXOS results were further combined, it could be found that, if the surfactant amount is low with a packing density smaller than the Zn atom density in the (0001) plane of wurtzite ZnO (0.1085 Å⁻²), SOS molecules move together and localize to match the wurtzite surface structure, while the 2D crystals nucleate and expand at the air-water interface. Polycrystalline NSs are more likely to be developed by nearby small single-crystalline domains. The introduction of more surfactants makes the monolayer packing closer to the wurtzite ZnO (0001) lattice, and larger crystalline domains can be formed with less SOS molecule movements. In addition, more anionic surfactants could enhance the electric field at the airwater interface and, thus, increase the supersaturation of Zn²⁺ ions to grow ZnO NSs. Therefore, the amount of surfactant can significantly influence the early nucleation kinetics in two ways: by determining the single-crystalline domain size by its packing density and by determining the interfacial Zn2+ concentration by its electrical double layer strength.

When the amount of surfactant was fixed, the NS nucleation and growth could also be influenced by the precursor metal ion concentration. As shown in Figure 4d-f, we can find that, with

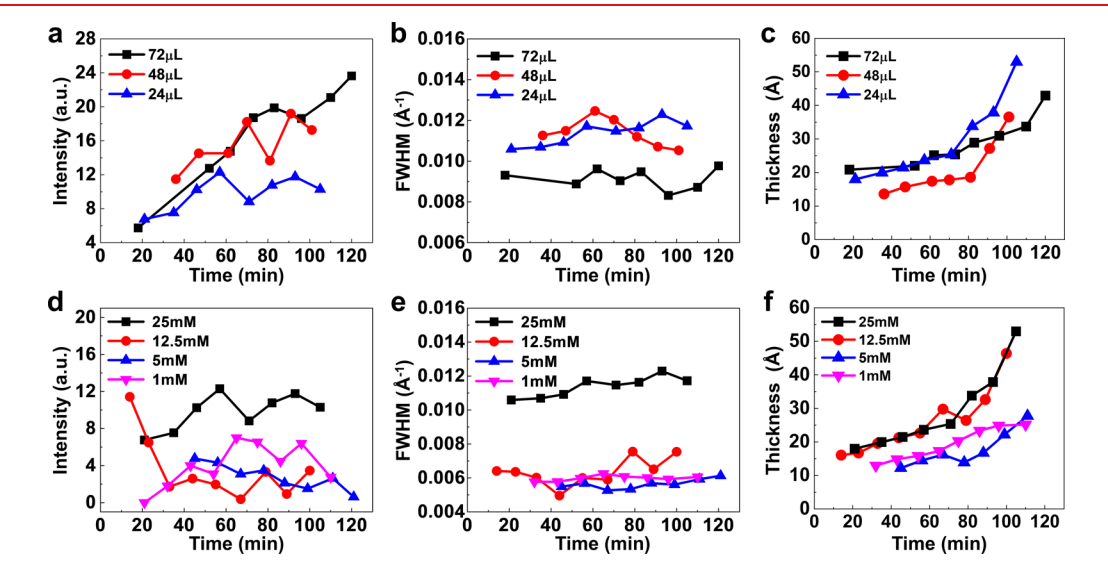


Figure 4. ZnO NS crystallinity and thickness changes at different growth conditions. (a) Diffraction rod (2D) intensity, (b) fwhm, and (c) nanosheet thickness evaluation as a function of growth time under different surfactant amounts [measurements were done at $60 \,^{\circ}$ C with 25 mM Zn²⁺]; (d) diffraction rod (2D) intensity, (e) fwhm, and (f) nanosheet thickness evaluation as a function of growth time at different Zn²⁺ concentrations [measurements were done at $60 \,^{\circ}$ C with 24 mL of SOS].

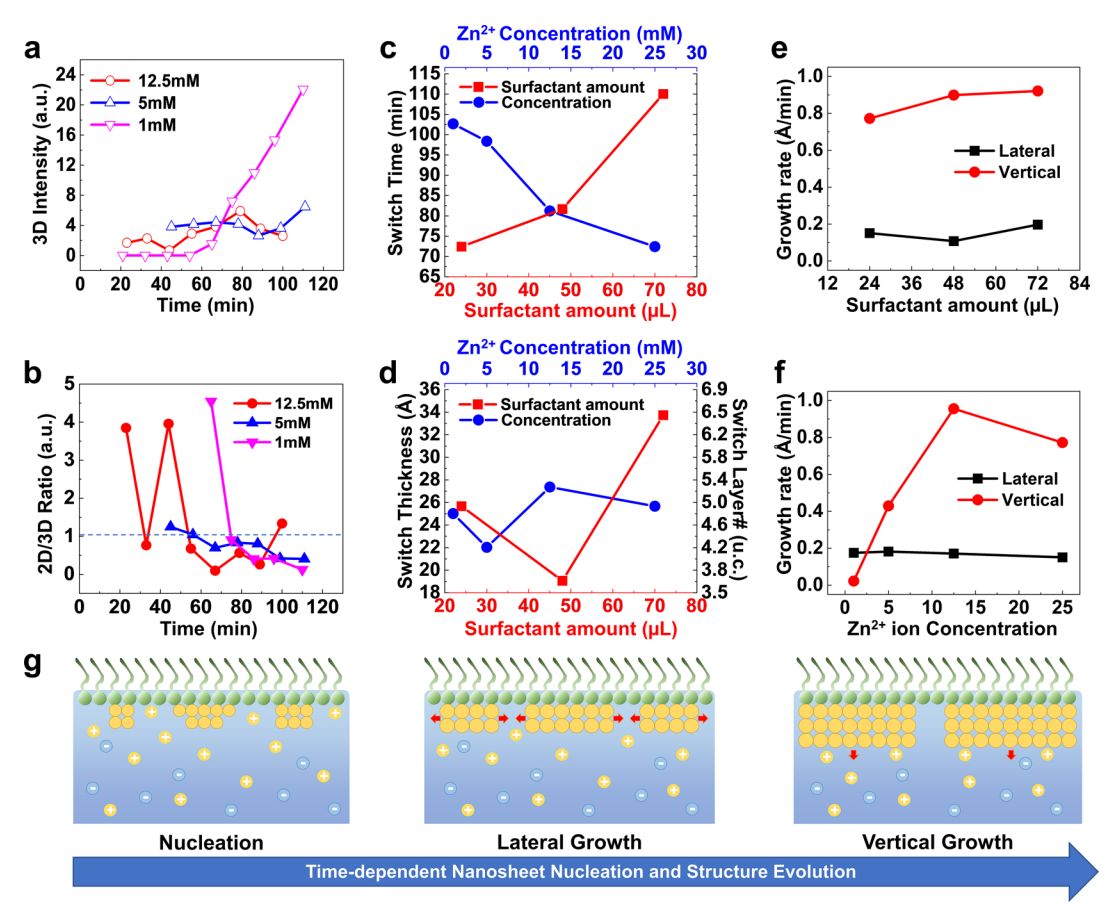


Figure 5. (a) Diffraction intensity of the diffraction ring (3D, $Q_{xy} = 2.224 \text{ Å}^{-1}$) at different Zn^{2+} concentrations. (b) Intensity ratios between 2D and 3D diffraction peaks [measurements were done at 60 °C with 24 mL of SOS]. (c) Critical switch time and (d) switch thickness at the lateral–vertical growth switch point for different conditions. Nanosheet thickness change rates in lateral and vertical growth for (e) different surfactant amounts and (f) different Zn^{2+} concentrations. (g) Schematic illustration of the nanosheet nucleation and structure evolution during the growth.

the same surfactant monolayer density, the intensity of the diffraction rod reached the plateau in a short period. Higher Zn²⁺ concentration accelerated the growth of NS thickness, but faster growth limited the alignment of the nuclei, leading to smaller average domain sizes. A 25 mM sample had a similar thickness increase as that of 12.5 mM, but it has more small crystalline domains, indicating it had a larger number of the initial nuclei, which might limit the single NS size during the growth. On the other hand, when the concentration was as low as 1 mM, the NS thickness only showed the first slow growth stage. This is likely due to the limited supply of Zn²⁺ precursor and thus makes the layer-by-layer growth unfavorable.

The relation between the rod and ring diffraction pairs from in situ GID and GIXOS disclosed an obvious 2D to 3D structure evolution in the ILE NS growth. Except for the highest Zn²+ concentration (25 mM), GID detected a diffraction ring @2.224 Å from all samples synthesized with other Zn²+ concentrations, and these intensities are shown in Figure 5a. The 1 mM sample showed the earliest and fastest rise of the 3D diffraction intensity, and this behavior was suppressed by increasing the precursor concentration. A high concentration is more favorable for attracting more precursors to the air—water interface, which is beneficial to the 2D nucleation and NS growth. The 2D–3D intensity ratios were calculated for samples at 12.5 mM Zn²+ concentration and below. As shown in Figure 5b, the 2D–3D intensity ratio from

higher Zn²⁺ concentrations decreased below 1 quicker, suggesting a faster formation of the bulk phase.

We further analyzed the thickness changing profiles obtained from GIXOS to shed light on the 2D to 3D crystal evolution. In the earlier slow stage, 2D nucleation and the thin interfacial epitaxy layer growth are dominant (lateral growth), and in the later fast stage, ZnO NSs grow thicker layer-by-layer (vertical growth). The critical time and thickness at the switching point between the two stages were plotted for different surfactant amounts and Zn²⁺ concentrations (Figure 5c,d). Longer switching times with smaller switching thicknesses were obtained from higher surfactant densities. This is because the 2D growth adapts surfactant on the NS surface, thereby reducing the surfactant density in the uncovered air-water interface area and eventually restricting further 2D growth. As a result, a larger surfactant quantity favored the longer-time 2D growth. A larger switching thickness occurred at 72 µL when the surfactant density was higher than the Zn atom density in (0001). This might be induced by a nonflat layer with extra surfactants, where the repulsion between surfactant molecules became significant.²⁷ An increase in precursor ion concentration reduced the switching time but without obvious changes to the switching thickness. This also confirmed that the lateral growth was mainly controlled by the amount of surfactant. Altogether, the switching thickness was determined by the packing density of the surfactants, and the switching time was more correlated to Zn²⁺ concentrations, where a

higher concentration raised the ion flux to the interfacial growth sites and suppressed 2D to 3D switching.

The slopes of the linear regions in these two stages were fitted to provide the thickness change rates in Figure 5e,f. The thickness change rates in the lateral growth stage had a similar changing trend as their corresponding switching thickness changes. This further proves the significant role of the surfactant amount in the lateral growth stage. However, the amount of surfactant did not show notable influences on the vertical growth, since the surface charges were screened out by the first few ZnO layers. The influence of the Zn2+ concentration was manifested in the later stage by controlling the layered growth rate. Higher concentrations could induce faster growth of the new layers. Supported by all in situ observations, the ILE NS growth mechanism can be concluded. As illustrated in Figure 5g, before observable crystallites, there is an incubation stage when Zn2+ ions are attracted by the ionized surfactant head groups and concentrated in the electrical double layer to nucleate. In the lateral growth stage, 2D nuclei laterally grow and attach following the epitaxial modulation of the surfactant monolayer at the water-air interface until the surfactant charges are mostly screened. Eventually, in the vertical growth stage, NWs grow along the thickness direction via a layer-by-layer mode.

In summary, using an in situ ILE growth apparatus, we successfully performed time-resolved grazing incidence synchrotron X-ray scattering techniques during the growth of 2D ZnO NSs at the water-air interface. Fast observations of both in-plane and out-of-plane crystal growth were achieved with a time resolution of only a few minutes by applying GID and GIXOS techniques, allowing direct observation of the 2D crystal nucleation and growth processes with a unit-cell resolution. We discovered an obvious lattice deformation in the first two surface layers, which is different from the inner bulk phase. This discovery of surface strain in ILE may open a new route toward strain-induced physical property tuning of 2D nanomaterials by surfactant engineering. We also evidenced the significance of the surfactant monolayer in the three stages of ILE NS growth. In addition, we show the impacts of different synthesis parameters on the NS growth behavior. Higher surfactant density enhanced the effects of the electrical double layer extending the lateral growth period, and higher Zn²⁺ concentration accelerated the 2D crystal growth, which are both favorable for large NS morphology formation. These results provide fundamental insights into the surfactanttemplated 2D growth mechanism in the ILE NS synthesis. The successful in situ diffraction characterization expands the toolbox to reveal the fast crystal nucleation and growth kinetics at the liquid interfaces by using time-resolved grazing incidence X-ray scattering techniques.

ASSOCIATED CONTENT

Supporting Information

The Supporting Information is available free of charge at https://pubs.acs.org/doi/10.1021/acs.nanolett.2c00300.

Section 1, experimental section; Section 2, GID data processing method; Section 3, nanosheet thickness calculation from fitting the periodicity of the GIXOS curve; Section 4, packing density calculation at the air—water interface; Section 5, temperature effects in ILE ZnO NS growth (PDF)

AUTHOR INFORMATION

Corresponding Author

Xudong Wang — Department of Materials Science and Engineering, University of Wisconsin-Madison, Madison, Wisconsin 53706, United States; orcid.org/0000-0002-9762-6792; Email: xudong.wang@wisc.edu

Authors

Ziyi Zhang — Department of Materials Science and Engineering, University of Wisconsin-Madison, Madison, Wisconsin 53706, United States; orcid.org/0000-0001-9102-8292.

Corey Carlos — Department of Materials Science and Engineering, University of Wisconsin-Madison, Madison, Wisconsin 53706, United States; orcid.org/0000-0002-9398-2554

Yizhan Wang — Department of Materials Science and Engineering, University of Wisconsin-Madison, Madison, Wisconsin 53706, United States; orcid.org/0000-0003-0464-6610

Yutao Dong — Department of Materials Science and Engineering, University of Wisconsin-Madison, Madison, Wisconsin 53706, United States; Occid.org/0000-0003-3582-087X

Xin Yin — Department of Materials Science and Engineering, University of Wisconsin-Madison, Madison, Wisconsin 53706, United States; Occid.org/0000-0002-4759-0226

Lazarus German — Department of Materials Science and Engineering, University of Wisconsin-Madison, Madison, Wisconsin 53706, United States; orcid.org/0000-0002-8573-5203

Kelvin Jordan Berg — Department of Materials Science and Engineering, University of Wisconsin-Madison, Madison, Wisconsin 53706, United States

Wei Bu — NSF's ChemMatCARS, Pritzker School of Molecular Engineering, University of Chicago, Chicago, Illinois 60637, United States; orcid.org/0000-0002-9996-3733

Complete contact information is available at: https://pubs.acs.org/10.1021/acs.nanolett.2c00300

Author Contributions

Z.Z., X.Y., and X.W. conceived the project and designed the experiments. Z.Z. and X.Y. designed and built the growth chamber. Z.Z., Y.W., C.C., Y.D., W.B., and K.J.B. carried out the *in situ* experiments at APS. Z.Z. conducted the SEM characterizations. Z.Z. and L.G. analyzed and proposed the nucleation and growth kinetic models. Z.Z. performed the GID and GIXOS data processing and wrote the manuscript. X.W. supervised the project. All authors discussed the results and have given approval to the final version of the manuscript.

Notes

The authors declare no competing financial interest.

ACKNOWLEDGMENTS

This work was primarily supported by the National Science Foundation DMR-2114931. GID and GIXOS data was collected at NSF's ChemMatCARS Sector 15, which was principally supported by the Divisions of Chemistry (CHE) and Materials Research (DMR), National Science Foundation, under Grant NSF/CHE-1834750. The use of the Advanced Photon Source, an Office of Science User Facility operated for

the U.S. Department of Energy (DOE) Office of Science by Argonne National Laboratory, was supported by the U.S. DOE under Contract DE-AC02-06CH11357.

REFERENCES

- (1) Zhang, H. Ultrathin two-dimensional nanomaterials. *ACS Nano* **2015**, *9*, 9451–9469.
- (2) Geim, A. K.; Novoselov, K. S. In Nanoscience and technology: a collection of reviews from nature journals; World Scientific, 2010; pp 11–19.
- (3) Yin, X.; et al. Memristive behavior enabled by amorphous-crystalline 2D oxide heterostructure. *Adv. Mater.* **2020**, 32, 2000801.
- (4) Guan, M.; et al. Vacancy associates promoting solar-driven photocatalytic activity of ultrathin bismuth oxychloride nanosheets. *J. Am. Chem. Soc.* **2013**, *135*, 10411–10417.
- (5) Ma, R.; et al. Topochemical synthesis of monometallic (Co2+-Co3+) layered double hydroxide and its exfoliation into positively charged Co (OH) 2 nanosheets. *Angew. Chem., Int. Ed.* **2008**, 47, 86–89.
- (6) Wang, Y.; et al. Bioinspired Synthesis of Quasi-Two-Dimensional Monocrystalline Oxides. *Chem. Mater.* **2019**, *31*, 9040–9048.
- (7) Wang, Y.; Zhang, Z.; Mao, Y.; Wang, X. Two-dimensional nonlayered materials for electrocatalysis. *Energy Environ. Sci.* **2020**, *13*, 3993–4016.
- (8) Tan, C.; Zhang, H. Wet-chemical synthesis and applications of non-layer structured two-dimensional nanomaterials. *Nat. Commun.* **2015**, *6*, 7873.
- (9) Meron, M.; Gebhardt, J.; Brewer, H.; Viccaro, J.; Lin, B. Following transient phases at the air/water interface. *European Physical Journal Special Topics* **2009**, *167*, 137–142.
- (10) Dai, Y.; et al. A comparative study of Langmuir surfactant films: Grazing incidence x-ray off-specular scattering vs. x-ray specular reflectivity. *J. Appl. Phys.* **2011**, *110*, 102213.
- (11) Dai, Y.; et al. Synchrotron X-ray studies of rapidly evolving morphology of self-assembled nanoparticle films under lateral compression. *Langmuir* **2013**, *29*, 14050–14056.
- (12) Bu, W.; Schlossman, M. L. Synchrotron X-ray scattering from liquid surfaces and interfaces. Synchrotron Light Sources and Free-Electron Lasers: Accelerator Physics, Instrumentation and Science Applications 2020, 1897–1933.
- (13) Kjaer, K. Some simple ideas on x-ray reflection and grazing-incidence diffraction from thin surfactant films. *Physica B: Condensed Matter* **1994**, *198*, 100–109.
- (14) Wang, F.; et al. Nanometre-thick single-crystalline nanosheets grown at the water—air interface. *Nat. Commun.* **2016**, *7*, 10444.
- (15) Yan, G.; et al. Enhanced Ferromagnetism from Organic—Cerium Oxide Hybrid Ultrathin Nanosheets. *ACS Appl. Mater. Interfaces* **2019**, *11*, 44601–44608.
- (16) Yan, G.; et al. Nanoparticle-Decorated Ultrathin La 2 O 3 Nanosheets as an Efficient Electrocatalysis for Oxygen Evolution Reactions. *Nano-micro letters* **2020**, *12*, 49.
- (17) Yin, X.; et al. Ionic layer epitaxy of nanometer-thick palladium nanosheets with enhanced electrocatalytic properties. *Chem. Mater.* **2018**, *30*, 3308–3314.
- (18) Zhang, Z.; et al. In vitro study of enhanced photodynamic cancer cell killing effect by nanometer-thick gold nanosheets. *Nano Research* **2020**, *13*, 3217–3223.
- (19) Tian, P.; Yu, Y.; Yin, X.; Wang, X. A wafer-scale 1 nm Ni (OH) 2 nanosheet with superior electrocatalytic activity for the oxygen evolution reaction. *Nanoscale* **2018**, *10*, 5054–5059.
- (20) Wang, F.; Yu, Y.; Yin, X.; Tian, P.; Wang, X. Wafer-scale synthesis of ultrathin CoO nanosheets with enhanced electrochemical catalytic properties. *Journal of Materials Chemistry A* **2017**, *5*, 9060–9066
- (21) Tolan, M.; Press, W.; Brinkop, F.; Kotthaus, J. X-ray diffraction from laterally structured surfaces: Crystal truncation rods. *Journal of applied physics* **1994**, *75*, *7761*–*7769*.

- (22) Petukhov, A.; Dolbnya, I.; Aarts, D.; Vroege, G.; Lekkerkerker, H. Bragg rods and multiple X-ray scattering in random-stacking colloidal crystals. *Physical review letters* **2003**, *90*, 028304.
- (23) LaMer, V. K.; Dinegar, R. H. Theory, production and mechanism of formation of monodispersed hydrosols. *Journal of the American chemical society* **1950**, 72, 4847–4854.
- (24) De Yoreo, J. J.; Vekilov, P. G. Principles of crystal nucleation and growth. Reviews in mineralogy and geochemistry 2003, 54, 57–93.
- (25) Wang, F.; Yin, X.; Wang, X. Morphological control in the adaptive ionic layer epitaxy of ZnO nanosheets. *Extreme Mechanics Letters* **2016**, *7*, 64–70.
- (26) Wang, F.; Seo, J.-H.; Ma, Z.; Wang, X. Substrate-free self-assembly approach toward large-area nanomembranes. *ACS Nano* **2012**, *6*, 2602–2609.
- (27) Yin, X.; et al. Unit cell level thickness control of single-crystalline zinc oxide nanosheets enabled by electrical double-layer confinement. *Langmuir* **2017**, *33*, 7708–7714.

Recommended by ACS

Short-Range Order Tunes Optical Properties in Long-Range Disordered ZnSnN2-ZnO Alloy

Celeste L. Melamed, Adele C. Tamboli, et al.

APRIL 29, 2022

CHEMISTRY OF MATERIALS

READ 🗹

Short-Range Mechanisms in the Creation of a ZnO/InGaAs Interface

Gianluca Ciatto, Hubert Renevier, et al.

JULY 05, 2022

CRYSTAL GROWTH & DESIGN

READ 🗹

Elucidating the Evolving Atomic Structure in Atomic Layer Deposition Reactions with in Situ XANES and Machine Learning

Orlando Trejo, Neil P. Dasgupta, et al.

NOVEMBER 04, 2019

CHEMISTRY OF MATERIALS

READ [7]

Phase Diagram for Twinning Superlattice Te-Doped GaAs Nanowires

Ara Ghukasyan, Ray R. LaPierre, et al.

JANUARY 28, 2022

NANO LETTERS

READ 🗹

Get More Suggestions >